INTERNATIONAL JOURNAL FOR NUMERICAL METHODS IN FLUIDS
Int. J. Numer. Meth. Fluids 2006; **52**:707–721
Published online 6 March 2006 in Wiley InterScience (www.interscience.wiley.com). DOI: 10.1002/fld.1196

Continuation of travelling-wave solutions of the Navier–Stokes equations

Isabel Mercader[‡], Oriol Batiste[*,†] and Arantxa Alonso[§]

Departament de Física Aplicada, Universitat Politècnica de Catalunya, Barcelona, Spain

SUMMARY

An efficient way of obtaining travelling waves in a periodic fluid system is described and tested. We search for steady states in a reference frame travelling at the wave phase velocity using a first-order pseudospectral semi-implicit time scheme adapted to carry out the Newton's iterations. The method is compared to a standard Newton–Raphson solver and is shown to be highly efficient in performing this task, even when high-resolution grids are used. This method is well suited to three-dimensional calculations in cylindrical or spherical geometries. Copyright © 2006 John Wiley & Sons, Ltd.

KEY WORDS: Navier–Stokes equations; travelling waves; numerical methods

1. INTRODUCTION

Travelling waves appear in fluid systems as a result of various types of hydrodynamic instabilities. For instance, many flows driven by shear stresses result in travelling wave patterns. Examples of such flows are the Tollmien–Schlichting waves in the Poiseuille flow [1], and the precessing vortex breakdown solutions generated in a cylinder by the differential rotation of the end walls [2–4]. Travelling waves are also observed in systems in which thermal instabilities play an important role. This is the case of the travelling convection rolls induced in annular or circular domains by double diffusion effects [5], or the thermal Rossby waves in rotating systems [6], which usually arise in geophysical flows and play a fundamental role in weather and climate evolution.

Performing a time integration of the Navier–Stokes equations only permits the computation of the stable TW branches of solutions. However, unstable travelling waves, as well as

*Correspondence to: O. Batiste, Departament de Física Aplicada, Universitat Politècnica de Catalunya, Barcelona, Spain.
†E-mail: oriol@fa.upc.edu
‡E-mail: isabel@fa.upc.edu
§E-mail: arantxa@fa.upc.edu

Contract/grant sponsor: DGCYT; contract/grant number: BFM2003-00657

Received 4 July 2005
Revised 2 January 2006
Accepted 8 January 2006

unstable steady states, usually play a fundamental role in the understanding of fluid dynamical processes. The continuation of full branches of travelling waves is thus of fundamental importance to thoroughly understand the origin of the dynamics observed in spatially periodic systems.

Uniform trains of travelling waves can only exist in systems with a translational or a rotational symmetry. In such systems, it is possible to choose a reference frame moving or rotating at the wave phase velocity, which is unknown *a priori*, and to solve for a steady state. Proceeding in this way, the computation of travelling waves requires the resolution of the nonlinear equations with a Newton-like solver, and is not more difficult than that of steady states. In addition, both stable and unstable travelling-wave solutions can be obtained. This approach has been used in the study of Rayleigh–Bénard convection [7] and in the analysis of Poiseuille flow [1], among other problems.

Recently, much more efficient methods for the computation of steady states of the Navier–Stokes equations have been introduced. These methods make use of a first-order semi-implicit time scheme for the calculation of a Stokes preconditioner, which allows a matrix-free inversion of the preconditioned Jacobian. This idea can be straightforwardly applied to the computation of travelling waves, provided that the new terms arising from the change in the frame of reference are properly treated in the time-stepping algorithm. In this paper, we will show a way of doing this and we will compare the method to a standard Newton–Raphson solver with an explicit evaluation and inversion of the unpreconditioned Jacobian.

As it will be detailed below, these two methods are implemented in different formulations of the Navier–Stokes equations. The first one is implemented in a primitive variable formulation by using two different time-stepping methods, whereas the Newton–Raphson solver is applied in a stream-function formulation. It must be remarked that the matrix-free inversion of the preconditioned Jacobian could also be used in a stream-function formulation; however, we have chosen to implement it in a primitive variable formulation because it can be easily extended to three-dimensional problems.

We have applied the method to the calculation of TW branches in two-dimensional binary-fluid convection by using spectral techniques. Unlike convection in a pure fluid, the primary instability in binary mixtures when heated from below can be oscillatory. For sufficiently negative separation ratio a branch of TW originates at a subcritical Hopf bifurcation and acquires stability in a secondary saddle-node bifurcation. These TW are observed in experiments in large narrow rectangular and annular cells [5]. We will obtain the branch of TW and compare the efficiency of different methods in the computation of this TW solution.

The paper is organized as follows. In Section 2, we introduce a change of variables to obtain a steady system of equations and describe a way of solving efficiently the resulting system, as an alternative to the classical Newton–Raphson (CNR) scheme. Section 3 deals with the description of the test problem we have considered. In Section 4, we present the spectral discretization and the time-stepping algorithms used, and a comparison of the convergence and efficiency of the different methods is established. The main conclusions of the study are summarized in Section 5.

2. COMPUTATION OF TRAVELLING WAVES

The calculations carried out in this paper are aimed at obtaining spatially periodic solutions of the Navier–Stokes equations travelling at a velocity c in the periodic direction x. Since

any variable χ depends on the coordinate x and time t as $\chi_{\mathrm{TW}}(x,y,z,t)=\chi_{\mathrm{TW}}(x-ct,y,z)$, letting $\tilde{x}=x-ct$ in the governing equations, the time derivative of χ in the associated evolution equation becomes $-c\partial_{\tilde{x}}\chi$. Thus, we obtain a steady system of equations in the new spatial coordinates $\tilde{x}$, y, and z. The unknown phase velocity c can be determined by adding an equation to fix the phase of the solution. To do this, we typically force the real or imaginary part of a Fourier azimuthal coefficient in a fixed point (r,z) to be zero. Special care must be taken in the selection of the coefficient and point to avoid that the value of the coefficient at that point was fixed by any symmetry of the solution. Once we have converted the evolution equations into a steady system, we can apply the standard procedures to solve these new equations. We propose that this new term receives the same numerical treatment as the advective nonlinear terms $\mathbf{u}\cdot\nabla\chi$, in the Navier–Stokes equations and in the rest of conservation equations.

We present here calculations using two different approaches. The first one consists in using a CNR iterative scheme with an explicit evaluation of the Jacobian. As is well known, the building, storage and inversion of the Jacobian matrix, which is usually bad conditioned, constitutes in general a difficult task with notable limitations mainly associated to the number of equations M. The cost of direct inversion is order $O(M^3)$, which is not improved if matrix-free methods are used as an alternative. However, since we use this approach in a stream-function formulation of the Navier–Stokes equations (the problem proposed as a test is two-dimensional), we have the advantage of avoiding the problems associated with the coupling of the pressure with the velocity to satisfy the incompressibility constraint. The solution of the discretized problem satisfies both the boundary conditions and the condition of incompressibility. We had previously used this method to calculate numerically the travelling waves arising in two-dimensional planar Poiseuille flow [1] and in Rayleigh–Bénard convection [7], and to obtain thermal Rossby waves [8].

The second approach, proposed by Mamun and Tuckerman [9], is based on solving in a very efficient manner the system resulting from each Newton iteration

$$(\mathbf{L}+\mathbf{N}_{\mathbf{X}})\delta\mathbf{X}=(\mathbf{L}+\mathbf{N})\mathbf{X} \tag{1a}$$

$$\mathbf{X}\leftarrow\mathbf{X}-\delta\mathbf{X} \tag{1b}$$

Here, $\mathbf{X}$ represents the spatially discretized fields, $\delta\mathbf{X}$ the correction fields in every Newton's iteration, $\mathbf{L}$ and $\mathbf{N}$ the spatially discretized linear and nonlinear operators, respectively, and $\mathbf{N}_{\mathbf{X}}$ the Jacobian of the nonlinear term evaluated at $\mathbf{X}$.

Mamun and Tuckerman noted that the first-order semi-implicit time scheme

$$\frac{\mathbf{X}^{n+1}-\mathbf{X}^{n}}{\Delta t}=\mathbf{L}\mathbf{X}^{n+1}+\mathbf{N}\mathbf{X}^{n} \tag{2}$$

where n stands for the instant of time, $t_{n+1}=t_n+\Delta t$, can be rewritten as

$$\frac{\mathbf{X}^{n+1}-\mathbf{X}^{n}}{\Delta t}=(\mathbf{I}-\Delta t\mathbf{L})^{-1}(\mathbf{L}+\mathbf{N})\mathbf{X}^{n} \tag{3}$$

They proposed to solve the linear system (1a) in every Newton's iteration using $\mathbf{P}=(\mathbf{I}-\Delta t\mathbf{L})^{-1}$, with a large value of Δt, as a preconditioner,

$$(\mathbf{I}-\Delta t\mathbf{L})^{-1}(\mathbf{L}+\mathbf{N}_{\mathbf{X}})\delta\mathbf{X}=(\mathbf{I}-\Delta t\mathbf{L})^{-1}(\mathbf{L}+\mathbf{N})\mathbf{X} \tag{4}$$

and to solve this linear system by using a matrix-free method. According to the relationship (3), the right-hand side of (4) can be obtained by carrying out a time step evolution, and the left-hand side by carrying out a linearized time step. In this way, neither the building of the Jacobian matrix $(\mathbf{L}+\mathbf{N}_{\mathbf{X}})$ nor its storage are needed. A summary of different problems in which this method was used to calculate steady solutions can be found in Reference [10].

We have implemented this second approach by using two different time-stepping methods. In these methods, the decoupling of the velocity and pressure is obtained from a specific splitting of the system based on the time integration scheme, where the pressure is determined by projecting an appropriate velocity field into a divergence-free space.

The first fractional step method we have used was proposed by Karniadakis *et al.* [11] (hereafter referred to as KIO) and consists of an explicit treatment of the predicted velocity from the advection terms, followed by an implicit resolution of the corrected velocity from the diffusion terms. To solve the Poisson equation for the pressure, the authors introduce a Neumann boundary condition, obtained from the semi-discrete Navier–Stokes and continuity equations, which avoids instabilities. In this boundary condition the viscous linear term is rewritten in terms of a solenoidal part, approximated by an explicit scheme, and an irrotational part, approximated by an implicit scheme of appropriate order. This time-stepping scheme, modified as described in Reference [9], was used to compute steady states in a Marangoni convection problem in a differentially heated binary mixture [12].

The second time-stepping method we have used was proposed by Hugues and Randrimiampianina [13] (hereafter referred to as IPS) and corresponds to an improvement of the projection scheme proposed by Goda [14] and implemented by Gresho [15] to finite element approximations. The fractional steps consists of a predictor for the pressure, directly derived from the Navier–Stokes equations with the Neumann boundary condition proposed in Reference [11], a predictor for an intermediate velocity field from the momentum equation taking into account the predicted pressure obtained from the previous time level, and finally a correction step with an explicit evaluation of the final divergence-free velocity field. We have used this method in a second-order time-integration scheme to analyse two-dimensional oscillatory binary-fluid convection, both in large aspect ratio containers heated from below [16] and in laterally heated cavities [17]. In this last problem, a first-order time-stepping formulation to carry out Newton's method, as described above, was used to calculate the steady solutions [18].

3. THE TEST PROBLEM

We will test the different approaches in a problem of double-diffusive convection that gives rise to travelling waves in the first stage of convection. We consider Boussinesq binary-fluid convection in a two-dimensional domain $(x,z)\in[0,L]\times[0,d]$, with aspect ratio of the cell Γ defined as $\Gamma=L/d$, in the presence of a vertical gravity field $\mathbf{g}=-g\hat{\mathbf{e}}_z$. A vertical temperature gradient is imposed by fixing a temperature difference ΔT between the horizontal plates, with the temperature at the bottom higher than at the top. The boundary conditions are taken to be periodic in x, with period L, and we impose no mass flux, fixed temperature and the no-slip condition at the top and bottom plates. With these conditions the system admits the following basic conductive state, with constant gradients of temperature and concentration,

$$\mathbf{u}_c=0 \tag{5a}$$

$$T_c = T_0 - \Delta T\left(\frac{z}{d} - \frac{1}{2}\right) \tag{5b}$$

$$C_c = C_0 + C_0(1 - C_0)S_T\Delta T\left(\frac{z}{d} - \frac{1}{2}\right) \tag{5c}$$

where $\mathbf{u} = (u, w)$ is the velocity field; T and C are the fields of temperature and concentration of the denser component, respectively; T_0 and C_0 are their mean values, and S_T is the Soret coefficient.

The dynamics of the system is governed by the continuity equation, the Navier–Stokes equations and the energy and mass conservation equations [19]. If we nondimensionalize the equations using the height of the layer d as the unit of length, the vertical thermal diffusion time d^2/κ (κ being the thermal diffusivity), as the unit of time and the imposed vertical temperature difference ΔT as the unit of temperature, the dimensionless equations in the Boussinesq approximation read as follows

$$\nabla \cdot \mathbf{u} = 0 \tag{6a}$$

$$\partial_t \mathbf{u} + (\mathbf{u} \cdot \nabla)\mathbf{u} = -\nabla p + \sigma\nabla^2\mathbf{u} + R\sigma[(1 + S)\Theta + S\eta]\hat{\mathbf{e}}_z \tag{6b}$$

$$\partial_t \Theta + (\mathbf{u} \cdot \nabla)\Theta = w + \nabla^2\Theta \tag{6c}$$

$$\partial_t \eta + (\mathbf{u} \cdot \nabla)\eta = -\nabla^2\Theta + \tau\nabla^2\eta \tag{6d}$$

Here, Θ denotes the departure of temperature from its conduction profile, $\Theta = (T - T_c)/\Delta T$, and η is related to the concentration and temperature as $\eta = -(C - C_c)/(C_0(1 - C_0)S_T\Delta T) - \Theta$. The dimensionless parameters in the above equations are the Rayleigh number R, the Prandtl number σ, the Lewis number τ, and the separation ratio S, defined as

$$R = \frac{\alpha\Delta T g d^3}{\kappa\nu}, \quad \sigma = \frac{\nu}{\kappa}, \quad \tau = \frac{D}{\kappa}, \quad S = C_0(1 - C_0)\frac{\beta}{\alpha}S_T$$

where α and β are the thermal and concentration expansion coefficients, ν is the kinematic viscosity and D is the mass diffusivity. The boundary conditions at the top and bottom plates are

$$\mathbf{u} = \Theta = \partial_z\eta = 0 \quad \text{on } z = 0, 1 \tag{7}$$

As a measure of the heat transport by convection, we use the Nusselt number Nu, defined as the ratio of the heat flux through the top plate to that of the corresponding conductive solution. It has the following expression:

$$Nu = 1 - \Gamma^{-1}\int_{x=0}^{x=\Gamma} \partial_z\Theta(z = 1)\,\mathrm{d}x$$

We also evaluate, as an estimate of the strength of the convection, the dimensionless quantity E_k, defined as

$$E_k = \Gamma^{-1}\int_{x=0}^{x=\Gamma}\int_{z=0}^{z=1} \mathbf{u} \cdot \mathbf{u}\,\mathrm{d}x\,\mathrm{d}z$$

which is directly related to the mean kinetic energy of the system.

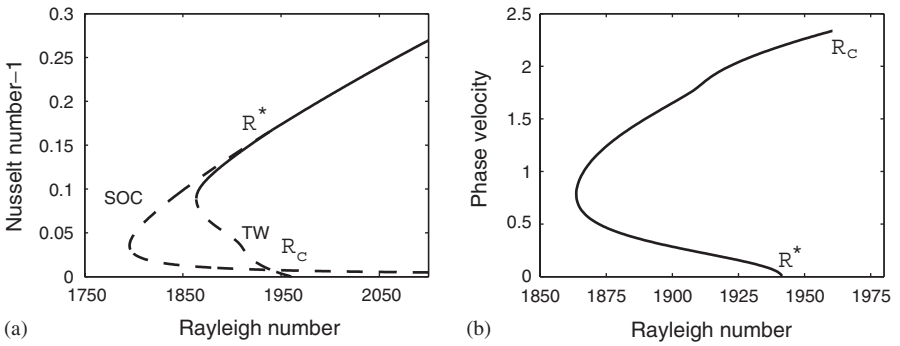

Figure 1. (a) Bifurcation diagram (Nusselt number − 1 versus the Rayleigh number) showing the SOC and TW branches of solutions in a periodic box of $\Gamma = 2$; and (b) phase velocity of the TW as a function of the Rayleigh number. R^* indicates the parity-breaking bifurcation of the SOC states and R_c the Hopf bifurcation of the conductive state. $S = -0.12$, $\sigma = 6.86$, $\tau = 0.0083$.

For sufficiently negative values of the separation ratio, which is the case considered here, the onset of convection is oscillatory and the translation invariance is broken, i.e. the wave number k of the dominant perturbation is nonzero, and a pattern of wavelength $a = 2\pi/k$ appears. Due to the $O(2) \times \mathbf{Z}_2$ symmetries of the problem, the Hopf bifurcation of the conductive state gives rise to two branches of nontrivial solutions that bifurcate simultaneously [20]. The instability evolves either to a pattern of standing waves (SW) or into waves that travel in either x-direction (TW). For the parameters chosen in this paper, if we use the Rayleigh number as a bifurcation parameter, the TW branch typically bifurcates subcritically (see Figure 1), acquiring stability at a secondary saddle-node bifurcation. When the Rayleigh number is increased from the saddle-node point, the TW branch disappears in a parity-breaking bifurcation of steady solutions, usually called SOC states (stationary overturning convection), to which stability is transferred [21]. The standing waves are unstable from the onset and usually disappear in a global bifurcation in which the SW solution connects with an unstable SOC state.

Figure 1(a) shows the bifurcation diagram of solutions in a periodic box of $\Gamma = 2$ for $S = -0.127$, $\sigma = 6.86$, and $\tau = 0.0083$. The Nusselt number has been plotted as a function of the Rayleigh number, which is the control parameter of the system. The diagram includes the branches of travelling waves (TW) and steady-state solutions (SOC). Since for periodicity $\Gamma = 2$ the critical wavenumber is π, which is near the critical wavenumber in an infinite domain, only a pair of rolls fits in the box. As usual, dashed and solid lines denote unstable and stable solutions, respectively. As for the precise location of the bifurcations presented in the diagram, the critical Rayleigh number at the onset of convection is $R_c = 1960.5$, the Rayleigh number at which the secondary stabilizing saddle-node bifurcation in the TW branch takes place is $R_{\mathrm{SN}}^{\mathrm{TW}} = 1863.7$, the Rayleigh number of the saddle-node bifurcation in the SOC branch is $R_{\mathrm{SN}}^{\mathrm{SOC}} = 1795.8$ and the Rayleigh number of the parity-breaking bifurcation in which the TW branch disappears and transfers stability to the SOC solution is $R^* = 1941.5$. In Figure 1(b) we have depicted the phase velocity of the travelling waves as a function of the Rayleigh number. At R_c the phase velocity is $c = 2.337$ and at R^* goes to zero, as corresponds to the parity-breaking bifurcation of the SOC states that takes place there. The structure of

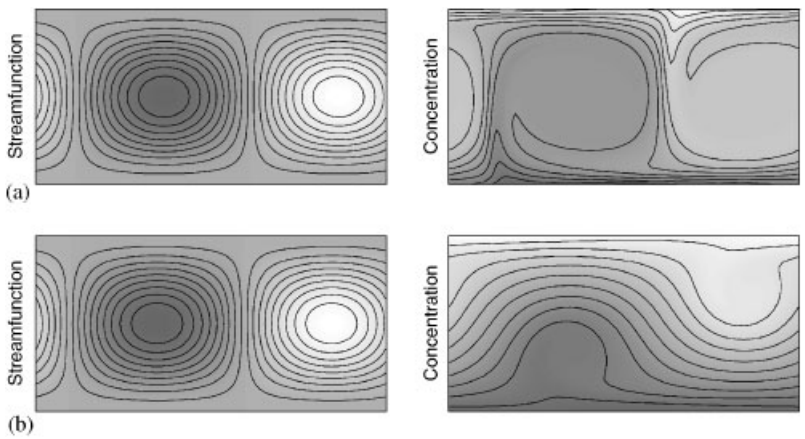

Figure 2. Streamlines and contour plots of the concentration field for the two TW solutions that exist at $R = 1900$ in a periodic box of $\Gamma = 2$. The solution plotted in: (a) belongs to the upper branch; and (b) to the lower branch. $S = -0.12$, $\sigma = 6.86$, $\tau = 0.0083$.

the TW, which is shown in Figure 2, and of the SOC states has been discussed extensively in References [21, 22].

4. DESCRIPTION AND COMPARISON OF THE DIFFERENT METHODS

In this section we present a comparison between the three methods presented in Section 2, CNR, KIO and IPS, when the two travelling waves that exist at a Rayleigh number $R = 1900$ for the parameters of Figure 1 are calculated. It should be noted that the solution belonging to the upper part of the TW branch is highly nonlinear and that, even though the temperature and velocity fields are nearly harmonic in the x-direction, the horizontal concentration profile has a trapezoidal shape [21, 22]. As a consequence, a high spatial resolution is required to resolve the narrow concentration boundary layers of these solutions. For the solution belonging to the lower part of the branch all the fields are nearly harmonic, and such a large spatial resolution is not needed. The streamlines and the contour plots of the concentration field of these two travelling waves, which are plotted in Figure 2, show this feature.

4.1. The CNR method

To obtain the stream-function formulation we proceed as follows. We split the solenoidal velocity field $\mathbf{u}(x, z, t)$ into its mean and fluctuating components,

$$\mathbf{u}(x, z, t) = \mathbf{U}(z, t) + \mathbf{u}'(x, z, t)$$

where $\mathbf{U} = (U, 0)$, $\mathbf{u}' = (-\partial_z \chi', \partial_x \chi')$ and $\overline{\mathbf{u}}' = \overline{\chi'} = 0$, with the overline indicating an average over the horizontal period.

Equations for U and χ' are obtained from the horizontal average of the Navier–Stokes equations and the deviation of the vorticity equation from its horizontal average. In the spatial

coordinates $\tilde{x} = x - ct$, y and z, the steady system of partial differential equations is

$$-\sigma\partial_{zz}^2 U + \partial_z \overline{u'_{\tilde{x}} u'_z} = 0 \tag{8a}$$

$$(-c\partial_{\tilde{x}} + U\partial_{\tilde{x}} - \sigma\nabla^2)\omega' + Ra\,\sigma[(1+S)\partial_{\tilde{x}}\Theta + S\partial_{\tilde{x}}\eta)]$$

$$+ \partial_{zz}^2 U\partial_{\tilde{x}}\chi' + \frac{\partial(\chi', \omega')}{\partial(\tilde{x}, z)} - \overline{\frac{\partial(\chi', \omega')}{\partial(\tilde{x}, z)}} = 0 \tag{8b}$$

$$(-c\partial_{\tilde{x}} + U\partial_{\tilde{x}} - \nabla^2)\Theta - \partial_{\tilde{x}}\chi' + \frac{\partial(\chi', \Theta)}{\partial(\tilde{x}, z)} = 0 \tag{8c}$$

$$(-c\partial_{\tilde{x}} + U\partial_{\tilde{x}} - \tau\nabla^2)\eta + \nabla^2\Theta + \frac{\partial(\chi', \eta)}{\partial(\tilde{x}, z)} = 0 \tag{8d}$$

where $\omega' = -\nabla^2\chi'$. The boundary conditions on $z = 0, 1$ become

$$U = \chi' = \partial_z\chi' = \Theta = \partial_z\eta = 0$$

The resulting problem is solved numerically using a spectral Galerkin–Fourier technique in $\tilde{x}$ and a collocation-Chebyshev method in z, by considering for U, χ', Θ, η the following expansions

$$U(z) = \sum_{m=1}^{N_z - 1} U_{km} f_m(2z - 1) \tag{9a}$$

$$\chi'(\tilde{x}, z) = \sum_{n=-N_x/2}^{N_x/2} \sum_{m=1}^{N_z - 3} \chi'_{nm} g_m(2z - 1) \mathrm{e}^{\mathrm{i}nk\tilde{x}} \tag{9b}$$

$$\theta(\tilde{x}, z) = \sum_{n=-N_x/2}^{N_x/2} \sum_{m=1}^{N_z - 1} \Theta_{nm} f_m(2z - 1) \mathrm{e}^{\mathrm{i}nk\tilde{x}} \tag{9c}$$

$$\eta(\tilde{x}, z) = \sum_{n=-N_x/2}^{N_x/2} \sum_{m=1}^{N_z - 1} \eta_{nm} h_m(2z - 1) \mathrm{e}^{\mathrm{i}nk\tilde{x}} \tag{9d}$$

where the functions $f_m(2z - 1)$, $g_m(2z - 1)$ and $h_m(2z - 1)$ are suitable combinations of Chebyshev polynomials satisfying the boundary conditions, and k is the wavenumber. The coefficients are forced to verify $a_{nm} = a^*_{-nm}$ ($*$ indicating complex conjugated), so that the fields are real. For every Fourier mode, equations have been written at the Gauss–Lobatto points $z_j = \cos \pi j / N_z$, with $j = 1, \ldots, N_z - 1$ for Equations (8a)–(8d) and with $j = 2, \ldots, N_z - 2$ for Equation (8b). The system of nonlinear equations resulting from the application of spectral methods is solved with a standard library routine that uses a modified Powell hybrid method.

In Tables I and II we show, for travelling waves belonging to the lower and upper branch, respectively, the values of the Nusselt number minus one, the phase velocity c and the mean kinetic energy E_k defined above, obtained with different spatial resolutions. Note that for the lower branch, convergence is reached with $N_x = 48$ horizontal mesh points (the results for $N_x = 48$, $N_z = 40$ and $N_x = 56$, $N_z = 40$ coincide). The figures of the solution obtained with $N_x = 48$, $N_z = 44$ do not vary if the resolution is increased. Table II shows that for the solution

Table I. Classical Newton–Raphson iterative method. $R = 1900$, lower part of the TW branch.

N_x	N_z	$Nu - 1$	c	E_k
36	18	0.0447172	1.6495707	2.191469
48	24	0.0445509	1.6512692	2.183347
48	32	0.0446342	1.6504908	2.187422
48	40	0.0446388	1.6504473	2.187647
56	40	0.0446388	1.6504473	2.187647
48	44	0.0446391	1.6504440	2.187664

Table II. Classical Newton–Raphson iterative method. $R = 1900$, upper part of the TW branch.

N_x	N_z	$Nu - 1$	c	E_k
36	18	0.1352568	0.2855636	6.640279
56	28	0.1352184	0.2842036	6.638087
64	28	0.1352186	0.2841876	6.638097
56	32	0.1352065	0.2846225	6.637482
64	32	0.1352067	0.2846077	6.637491
56	36	0.1352088	0.2845506	6.637601
56	42	0.1352084	0.2845618	6.637579

in the upper branch a bigger resolution in the x-direction (more than $N_x = 56$) is needed. Very likely, a spatial resolution of $N_z = 42$ in the z-direction is not enough either. Therefore, with the maximum resolution allowed by our computer, $N_x = 56$, $N_z = 42$, we cannot assert that all the figures of the quantities $Nu - 1$, c and E_k of the solution are exact. It is worth recalling that the solutions obtained with this method verify both the no-slip condition on the boundaries and the incompressibility condition.

4.2. The KIO method

In order to implement the first-order time-splitting method by using the KIO method [11], we have proceeded as follows.

- We obtain Θ^{n+1} from the Helmholtz-type problem

$$(\nabla^2 - \Delta t^{-1})\Theta^{n+1} = [(\mathbf{u} \cdot \nabla)\Theta - c\partial_{\tilde{x}}\Theta - w - \Theta/\Delta t]^n \tag{10}$$

  where the right-hand side contains quantities evaluated at the previous time step n. Boundary conditions are those specified in (7).
- Once Θ^{n+1} is known, we can obtain η^{n+1} from another Helmholtz-type problem

$$(\nabla^2 - (\tau\Delta t)^{-1})\eta^{n+1} = \tau^{-1}[(\mathbf{u} \cdot \nabla)\eta - c\partial_{\tilde{x}}\eta - \eta/\Delta t]^n + \tau^{-1}\nabla^2\Theta^{n+1} \tag{11}$$

  with the boundary conditions for η^{n+1} specified in (7).

- We combine the two equations

$$\frac{\hat{\mathbf{u}}-\mathbf{u}^n}{\Delta t} = -\nabla p - [(\mathbf{u}\cdot\nabla)\mathbf{u} - c\partial_{\tilde{x}}\mathbf{u}]^n + R\sigma[(1+S)\Theta^{n+1} + S\eta^{n+1}]\hat{\mathbf{e}}_z \tag{12a}$$

$$\nabla\cdot\hat{\mathbf{u}} = 0 \tag{12b}$$

  to obtain the Poisson equation for the pressure p. This equation is solved using a Neumann boundary condition derived from the semi-discrete Navier–Stokes equations and the incompressibility condition, where the diffusion is separated in a solenoidal part approximated by an explicit scheme of order one and in an irrotational part approximated by an implicit scheme. Once the pressure field is obtained, the solenoidal intermediate velocity field $\hat{\mathbf{u}}$ can be evaluated.
- Eventually, we obtain $\mathbf{u}^{n+1}$ from the following Helmholtz-type problem

$$(\nabla^2 - (\sigma\Delta t)^{-1})\mathbf{u}^{n+1} = -\hat{\mathbf{u}}/(\sigma\Delta t) \tag{13}$$

  which we solve with the correct boundary conditions for the velocity field.

For the spatial discretization we have used a Fourier–Galerkin spectral method in the x-direction (Fourier modes with wavenumber from 0 to $\pm N_x/2$) and a Chebyshev-collocation method in the z-direction. The advection terms have been obtained pseudospectrally calculating the products in $3N_x/2$ points of the physical space to avoid aliasing errors. Chebyshev Gauss–Lobatto collocation points $z_j = \cos \pi j/N_z$, with $j = 0, N_z$, are considered and all the derivatives in z have been calculated by matrix multiplication. In every step and for every Fourier mode n in x, we have solved in z a system of the type

$$(D_{zz} - a_n)\Phi_n(z) = h_n(z)$$

with boundary conditions in $z = 0, 1$. These systems are solved by using a diagonalization technique [23]. Finally, the linear system corresponding to the preconditioned version of Newton's iteration (4) has been solved with an iterative technique, using a GMRES package [24]. With this method the velocity field resulting from the final step $\mathbf{u}^{n+1}$ verifies the correct boundary conditions, but it is not forced to be solenoidal. To evaluate the deviation of the velocity field from the solenoidal character, we have introduced the variable 'div', which represents the mean divergence in the domain:

$$\mathrm{div} = \left[\Gamma^{-1}\int_{x=0}^{x=\Gamma}\int_{z=0}^{z=1}(\nabla\cdot\mathbf{u})^2\,\mathrm{d}x\,\mathrm{d}z\right]^{1/2}$$

Tables III and IV show the results obtained when the two travelling waves that exist at $R = 1900$ are calculated with different resolution. The value of the 'div' variable has also been included. In our computations the Newton's iteration finishes either when the norm of the right-hand side of Equation (4) is smaller than a certain small quantity ε_1 or when the relative error of the correction is small enough. Once the criterion of convergence is fixed, we have to choose the optimum Δt that allows to compute the solution with the minimum number of iterations at every step of the Newton iteration. An alternative criterion we have used to choose ε_1 and Δt is that 'div' be as small as possible for a given resolution. The solution obtained as a result of the Newton iteration can present some fluctuations depending

Table III. Preconditioned method using KIO integrator. $R = 1900$, lower part of the TW branch.

N_x	N_z	$Nu - 1$	c	E_k	div
36	18	0.042700	1.68771	2.09318	6.4×10^{-3}
48	24	0.044652	1.64907	2.18827	5.1×10^{-4}
48	32	0.0446446	1.650285	2.187929	3.8×10^{-5}
48	40	0.0446393	1.650436	2.187674	1.9×10^{-6}
56	40	0.0446393	1.650436	2.187674	1.9×10^{-6}
48	44	0.0446390	1.650446	2.187658	4.7×10^{-7}
48	60	0.0446390	1.650446	2.187657	2.0×10^{-7}

Table IV. Preconditioned method using KIO integrator. $R = 1900$, upper part of the TW branch.

N_x	N_z	$Nu - 1$	c	E_k	div
36	18	0.134413	0.29551	6.65984	4.0×10^{-3}
56	28	0.135192	0.2841670	6.63675	1.4×10^{-4}
64	28	0.135192	0.2841511	6.63676	1.4×10^{-4}
56	32	0.1352311	0.2845325	6.638707	1.1×10^{-4}
64	32	0.1352313	0.2845178	6.638716	1.1×10^{-4}
56	36	0.1351994	0.2845908	6.637134	4.2×10^{-5}
56	42	0.1352085	0.2845621	6.637585	8.0×10^{-7}
80	70	0.1352086	0.2845484	6.637590	3.0×10^{-8}

on the chosen value of Δt and ε_1. The results that appear in Tables III and IV, where only the significant figures have been included, are obtained with the values of Δt and ε_1 that give the minimum value of 'div'. We use typically $\varepsilon_1 \approx 10^{-9}$ and Δt between 100 and 1000. Note that the larger the resolution used, the smaller the value of 'div' that we obtain. By comparing with the results obtained with the first method, we see that the solutions at the lower branch converge quite well, and that if the resolution in z is increased we obtain the same result. The same occurs with the solution at the upper branch, but with this method we are able to further increase the resolution, since the Jacobian is not stored or inverted explicitly. We can see that the result with $N_x = 80$, $N_z = 70$ only presents small differences with respect to the solution obtained with $N_x = 56$, $N_z = 42$.

4.3. The IPS method

In this section, we detail the fractional steps in the first-order splitting method by using the improved projection scheme IPS proposed in Reference [13]. Note that the two first steps corresponding to obtaining Θ^{n+1} and η^{n+1} are the same as those at the KIO method.

- Θ^{n+1} is obtained from the Helmholtz-type problem

$$(\nabla^2 - \Delta t^{-1})\Theta^{n+1} = [(\mathbf{u} \cdot \nabla)\Theta - c\partial_{\tilde{x}}\Theta - w - \Theta/\Delta t]^n \tag{14}$$

  with the boundary conditions specified in (7).

- η^{n+1} is calculated solving

$$(\nabla^2 - (\tau\Delta t)^{-1})\eta^{n+1} = \tau^{-1}[(\mathbf{u}\cdot\nabla)\eta - c\partial_{\tilde{x}}\eta - \eta/\Delta t]^n + \tau^{-1}\nabla^2\Theta^{n+1} \tag{15}$$

  with the boundary conditions for η^{n+1} specified in (7).
- We obtain a preliminary pressure field from the Navier–Stokes and continuity equations

$$\nabla^2\bar{p}^{n+1} = \nabla\cdot\{[-(\mathbf{u}\cdot\nabla)\mathbf{u} + c\partial_{\tilde{x}}\mathbf{u}]^n + R\sigma[(1+S)\Theta^{n+1} + S\eta^{n+1}]\hat{\mathbf{e}}_z\} \tag{16}$$

  with the Neumann boundary condition from the pressure proposed in Reference [11].
- We calculate a predictor velocity field $\mathbf{u}^*$ from the Navier–Stokes equation by including the predictor pressure $\bar{p}$ with the actual boundary conditions

$$\begin{aligned}(\nabla^2 - (\sigma\Delta t)^{-1})\mathbf{u}^* = {} & \sigma^{-1}\nabla\bar{p}^{n+1} + \sigma^{-1}[(\mathbf{u}\cdot\nabla)\mathbf{u} - c\partial_{\tilde{x}}\mathbf{u} - \mathbf{u}/\Delta t]^n \\ & - R[(1+S)\Theta^{n+1} + S\eta^{n+1}]\hat{\mathbf{e}}_z\end{aligned}$$

- In the correction step we solve the system

$$\frac{\mathbf{u}^{n+1} - \mathbf{u}^*}{\Delta t} = -\nabla(p^{n+1} - \bar{p}^{n+1}) \tag{17a}$$

$$\nabla\cdot\mathbf{u}^{n+1} = 0 \tag{17b}$$

  with the first equation satisfied also on the boundary, and with the correct boundary condition for the normal component of the velocity field. This system gives rise to a Poisson equation for the variable $\Phi = \Delta t(p^{n+1} - \bar{p}^{n+1})$ with the Neumann boundary condition $\partial\Phi/\partial n = 0$. Eventually, the corrected pressure and velocity fields, p^{n+1} and $\mathbf{u}^{n+1}$, are calculated from the value of Φ

$$p^{n+1} = \bar{p}^{n+1} + \Phi/\Delta t \tag{18a}$$

$$\mathbf{u}^{n+1} = \mathbf{u}^* - \nabla\Phi \tag{18b}$$

For the spatial discretization we have used a Fourier-collocation method in x and a Chebyshev-collocation method in z. Collocation points in x are $x_i = 2\pi i/N_x$, with $i = 0, N_x - 1$, and in z the Chebyshev Gauss–Lobatto points $z_j = \cos\pi j/N_z$, with $j = 0, N_z$. All the derivatives in x and z have been calculated by matrix multiplication. On Fourier and Chebyshev-collocation points the Helmholtz and Poisson equations are solved by using complete diagonalization in both directions [23]. As in the KIO method, the linear system corresponding to the preconditioned version of Newton's iteration has been solved by using a GMRES package [24]. Note that with this method the velocity field $\mathbf{u}$ slips on the boundary, since only the normal component is forced to be zero in the correction step. As a measure of the deviation from the no-slip condition we have used the variable 'slip', defined as

$$\text{slip} = \left[\Gamma^{-1}\int_{x=0}^{x=\Gamma}[u(z=1)]^2\,\mathrm{d}x\right]^{1/2}$$

Table V. Preconditioned method using IPS integrator. $R = 1900$, upper part of the TW branch.

N_x	N_z	$Nu - 1$	c	E_k	slip
36	18	0.0436847	1.666722	2.141600	1.5×10^{-3}
48	24	0.0446268	1.650115	2.187020	1.1×10^{-3}
48	32	0.0446401	1.650397	2.187705	8.0×10^{-6}
48	40	0.0446391	1.650442	2.187662	4.0×10^{-6}
56	40	0.0446391	1.650443	2.187661	4.0×10^{-7}
48	44	0.0446391	1.650444	2.187662	1.0×10^{-7}
48	60	0.0446391	1.650445	2.187661	2.0×10^{-9}

Table VI. Preconditioned method using IPS integrator. $R = 1900$, upper part of the TW branch.

N_x	N_z	$Nu - 1$	c	E_k	slip
36	18	0.135245	0.27278	6.63903	9.5×10^{-4}
56	28	0.135208	0.28416	6.63675	3.3×10^{-5}
64	28	0.135207	0.28421	6.63753	3.2×10^{-5}
56	32	0.135216	0.28452	6.63801	2.5×10^{-5}
64	32	0.135211	0.28457	6.63796	1.2×10^{-5}
56	36	0.135205	0.28452	6.63741	8.0×10^{-6}
56	42	0.135209	0.28451	6.63761	2.0×10^{-7}
80	70	0.135208	0.28455	6.63758	5.0×10^{-8}

In Tables V and VI we show the results obtained when we calculate the two travelling waves that exist at $R = 1900$ with different resolution. We have also included the value of the 'slip' variable defined above. The criteria used to finish the Newton iterations are similar to those used in the KIO method, with the 'slip' variable playing the same role as the 'div' variable. As occurred there, the larger the resolution used, the smaller the value of 'slip' we obtain. By imposing the same value of ε_1, $\varepsilon_1 \approx 10^{-9}$, we have to use a bigger value of Δt than in the KIO method. However, with a lower resolution, the solution obtained with the IPS method seems to present less error than with the KIO method.

Finally, it is worth comparing the CPU running time with the three methods. We have measured the time devoted to calculating the solution at Rayleigh number $R = 1910$, giving as a guess the solution at Rayleigh number $R = 1900$. With a resolution of $N_x = 56$, $N_z = 42$, the CPU time with the CNR method is of about 25 min, whereas with the other methods the CPU time is of about 15 seconds. This information allows us to strongly recommend the usage of time-stepping codes for the preconditioning of the Newton's iterations to obtain travelling-wave solutions.

5. CONCLUSIONS

In this paper, a highly efficient way of obtaining travelling-wave solutions has been presented and tested in a two-dimensional binary-fluid convection problem. Travelling waves turn into

steady solutions when described from a reference frame moving at the wave phase velocity. Therefore, a simple change of variables allows us to obtain a stationary system of equations. To solve the resulting system, which includes the phase velocity as an unknown, we have followed two different approaches. In the first approach, we have implemented a classical Newton–Raphson (CNR) iterative scheme with an explicit evaluation of the Jacobian matrix, using spectral methods for the spatial discretization. Beforehand, since we have used a stream-function formulation of the Navier–Stokes equations, the solution of the discretized problem satisfies exactly both the boundary conditions and the incompressibility constraint. The known drawback of the method is the high cost of the construction, storage and inversion of the Jacobian matrix. In the second approach, we have used a method proposed by Mamun and Tuckerman [9] based on the adaptation of a time-stepping code to carry out each Newton's iteration. Here, we have implemented this method with two different fractional step techniques, the KIO and the IPS methods. Whereas in the KIO method the velocity field resulting from the final step verifies the boundary condition but is not forced to be solenoidal, just the opposite is the case with the velocity field in the IPS method. In both cases, it is important to treat properly in the time-stepping algorithm the new terms arising from the change in the frame of reference. An explicit treatment of these terms, similar to that of the nonlinear advective terms, allows us to maintain the structure of the time evolution solver unchanged and is shown to be effective for the calculations.

The careful analysis of the numerical tests made with the different methods leads to a number of interesting conclusions. First, the solutions obtained with the new method agree with those obtained with the stream-function formulation, showing that the splitting errors are not significant. It is important to emphasize that the values of the divergence in the IPS method and of the velocity slip in the KIO method become very small as the resolution is increased. It should also be noted that, although a very large value of the time step is used in the preconditioner, the final solution is not influenced by the error we should expect if this large value of the time step had been used in a time evolution with the same splitting scheme.

The second important conclusion is that the new method is extremely efficient if compared to the Newton–Raphson solver or to the direct computation of stable travelling waves with a time-stepping code. The CPU time needed to obtain a travelling-wave solution is reduced by two orders of magnitude with respect to the Newton–Raphson scheme.

Regarding the splitting scheme, our results show that the IPS method converges faster, for low resolutions, than the KIO scheme. Therefore, our method of choice would be the IPS splitting scheme combined either with a Galerkin or a collocation Fourier spectral method.

To summarize, in this paper we have described a practical and efficient way for the calculation of stable and unstable travelling waves in periodic geometries. This method is expected to be broadly applicable to problems in three-dimensional geometries, such as cylindrical, annular and spherical domains, where the first time-dependent solutions are usually in the form of travelling-waves. An existing time-dependent code based on a splitting algorithm can be easily adapted for the efficient computation of travelling-wave solutions.

ACKNOWLEDGEMENTS

We would like to thank DGCYT for financial support under grant BFM2003-00657.

REFERENCES

1. Drissi A, Net M, Mercader I. Subharmonic instabilities of Tollmien–Schlichting waves in two-dimensional Poiseuille flow. *Physical Review E* 1999; **60**:1781–1791.
2. Marques F, Lopez JM. Precessing vortex breakdown mode in an enclosed cylinder flow. *Physics of Fluids* 2001; **13**(6):1679–1682.
3. Lopez JM, Hart JE, Marques F, Kittelman S, Shen J. Precessing vortex breakdown mode in an enclosed cylinder flow. *Physics of Fluids* 2001; **13**(6):1679–1682.
4. Nore C, Tuckerman LS, Daube O, Xin S. The 1:2 mode interaction in exactly counter-rotating von Kármán swirling flow. *Journal of Fluid Mechanics* 2003; **477**:51–88.
5. Ohlsen DR, Yamamoto SY, Surko CM, Kolodner P. Transition from traveling-wave to stationary convection in fluid mixtures. *Physical Review Letters* 1990; **65**:1431–1434.
6. Or AC, Busse FH. Convection in a rotating cylindrical annulus. Part 2: transitions to asymmetric and vacillating flow. *Journal of Fluid Mechanics* 1987; **174**:313–326.
7. Prat J, Mercader I, Knobloch E. The 1:2 mode interaction in Rayleigh–Bénard convection with and without Boussinesq symmetry. *International Journal for Bifurcation and Chaos* 2002; **12**(2):281–308.
8. Pino D, Net M, Sánchez J, Mercader I. Thermal Rossby waves in a rotating annulus. Their stability. *Physical Review E* 2001; **63**(056312):1–14.
9. Mamun CK, Tuckerman LS. Asymmetry and Hopf bifurcation in spherical Couette flow. *Physics of Fluids* 1995; **7**:80–91.
10. Tuckerman LS, Barkley D. Bifurcation analysis for timesteppers. In *Numerical Methods for Bifurcation Problems and Large-scale Dynamical Systems*, Doedel E, Tuckerman LS (eds). Springer: Berlin, 2000; 453–466.
11. Karniadakis GE, Israeli M, Orszag SA. High order splitting methods for the incompressible Navier–Stokes equations. *Journal of Computational Physics* 1991; **97**:414–443.
12. Bergeon A, Henry D, Ben Hadid H, Tuckerman L. Natural doubly diffusive convection in binary mixtures with Soret effect. *Journal of Fluid Mechanics* 1998; **375**:143–177.
13. Hugues S, Randriamampianina A. An improved projection scheme applied to pseudospectral method for the incompressible Navier–Stokes equations. *International Journal for Numerical Methods in Fluids* 1998; **28**: 501–521.
14. Goda K. A multistep technique with implicit difference schemes for calculating two- and three-dimensional cavity flows. *Journal of Computational Physics* 1979; **30**:76–95.
15. Gresho P. On the theory of semi-implicit projection methods for viscous incompressible flow and its implementation via a finite element method that also introduces a nearly consistent mass matrix. Part I: theory. *International Journal for Numerical Methods in Fluids* 1990; **11**:587–620.
16. Batiste O, Net M, Mercader I, Knobloch E. Oscillatory binary fluid convection in large aspect-ratio containers. *Physical Review Letters* 2001; **81**(11):2309–2312.
17. Meca E, Mercader I, Batiste O, Ramírez-Piscina L. Blue sky catastrophe in double-diffusive convection. *Physical Review Letters* 2004; **93**(23):23450-1–23450-4.
18. Meca E, Mercader I, Batiste O, Ramírez-Piscina L. Complex dyanmics in double-diffusive convection. *Theoretical and Computational Fluid Dynamics* 2004; **18**:231–238.
19. Platten JK, Legros JC. *Convection in Liquids*. Springer: Berlin, Heidelberg, 1984.
20. Crawford JD, Knobloch E. Symmetry and symmetry-breaking bifurcations in fluid dynamics. *Annual Review of Fluid Mechanics* 1991; **23**:341–387.
21. Lücke M, Barten W, Büchel P, Fütterer C, Hollinger St, Jung Ch. In *Evolution of Spontaneous Structures in Dissipative Continuous Systems*, Busse FH, Müller SC (eds). Springer: Berlin, Heidelberg, 1998; 127–196.
22. Barten W, Lücke M, Kamps M, Schmitz R. Convection in binary fluid mixtures. I. Extended traveling-wave and stationary states. *Physical Review E* 1995; **51**:5636–5660.
23. Zaho S, Yedlin MJ. A new Iterative Chebyshev spectral method for solving the elliptic equation $\nabla \cdot (\sigma \nabla u) = f$. *Journal of Computational Physics* 1995; **113**:215–223.
24. Frayssé V, Giraud L, Gratton S, Langou J. A set of GMRES routines for real and complex arithmetics on high performance computers. *Technical Report TR/PA/03/3*, CERFACS; 2003. Public domain software available on www.cerfacs/algor/Softs.

